BBA - Bioenergetics 1859 (2018) 270–279

Contents lists available at ScienceDirect

BBA - Bioenergetics

journal homepage: www.elsevier.com/locate/bbabio

yVDAC2, the second mitochondrial porin isoform of *Saccharomyces cerevisiae*

Carlo Guardiani[a,1], Andrea Magrì[b,1], Andonis Karachitos[c,1], Maria Carmela Di Rosa[d], Simona Reina[d], Igor Bodrenko[e], Angela Messina[b], Hanna Kmita[c,*], Matteo Ceccarelli[e,*], Vito De Pinto[d,*]

[a] School of Engineering, University of Warwick, Coventry, UK
[b] Department of Biological, Geological and Environmental Sciences, Section of Molecular Biology, University of Catania, Italy
[c] Institute of Molecular Biology and Biotechnology, Faculty of Biology, Adam Mickiewicz University, Poznan, Poland
[d] Department of Biomedical and Biotechnological Sciences, University of Catania, Italy
[e] Department of Physics, University of Cagliari, Cagliari, Italy

ARTICLE INFO

Keywords:
Outer mitochondrial membrane (OMM)
Yeast VDAC isoforms
Molecular dynamics

ABSTRACT

The yeast *Saccharomyces cerevisiae* genome is endowed with two distinct isoforms of Voltage-Dependent Anion Channel (VDAC). The isoform yVDAC2 is currently understudied with respect to the best known yVDAC1. Yet, since the discovery, the function of yVDAC2 was unclear, leading to the hypothesis that it might be devoid of a channel function. In this work we have elucidated, by bioinformatics modeling and electrophysiological analysis, the functional activity of yVDAC2. The conformation of yVDAC2 and, for comparison, of yVDAC1 were modeled using a multiple template approach involving mouse, human and zebrafish structures and both showed to arrange the sequences as the typical 19-stranded VDAC β-barrel. Molecular dynamics simulations showed that yVDAC2, in comparison with yVDAC1, has a different number of permeation paths of potassium and chloride ions. yVDAC2 protein was over-expressed in the *S. cerevisiae* cells depleted of functional yVDAC1 (Δ*por1* mutant) and, after purification, it was reconstituted in artificial membranes (planar lipid bilayer (PLB) system). The protein displayed channel-forming activity and the calculated conductance, voltage-dependence and ion selectivity values were similar to those of yVDAC1 and other members of VDAC family. This is the first time that yVDAC2 channel features are detected and characterized.

1. Introduction

The Voltage Dependent Anion Channel (VDAC) is the major integral protein of the outer mitochondrial membrane and it acts as a permeability pathway for both inorganic ions, such as Ca^{2+}, Na^{+}, K^{+}, Cl^{-} or OH^{-}, and for organic metabolites, like ATP, ADP, NADH, pyruvate and succinate [1–3]. In mammals there are three VDAC isoforms encoded by three genes located on different chromosomes, showing the same exon-intron organization that testifies their comparatively recent common evolutionary origin [4,5]. The first structural model of VDAC channel was proposed by Colombini and co-workers, on the grounds of extensive electrophysiological measurements in conjunction with site-directed mutagenesis [6,7]. The resulting functional model was characterized by 13 β-strands and a transmembrane α-helix. Other models claimed for a 16 transmembrane β-strands, reminding the Gram-negative bacterial porins [8]. However, in 2008, three 3D-structures of mouse and human VDAC1 were resolved by means of X-ray crystallography and NMR [9–11]. The experimental structures revealed an unforeseen β-barrel motif with 19 β-strands, characterized by a regular alternation of inward-pointing hydrophilic residues and outward-pointing hydrophobic residues [9–11]. All the strands are organized in an anti-parallel arrangement but strands 1 and 19 that are parallel to one another [9–11]. This peculiar feature differentiates the VDAC channel from bacterial porins that follow the rule of a strictly even number of strands [12]. Another key element of VDAC channel is the α-helix-break-α-helix N-terminal end located inside the pore and possibly implicated in the gating mechanism [9–11]. Recently the same structural motif was discovered in a bacterial porin, CymA from *Klebsiella oxytoca* [13], and the recent resolution of the structure of zebrafish VDAC2 (at 2.80 Å resolution) revealed the same β-barrel motif of VDAC1 [14].

Alignment studies show that the main difference between the three mammalian VDAC isoforms is at the level of the N-terminus, that in VDAC1 and VDAC3 comprises the first 25 residues while in VDAC2 also

* Corresponding authors.
E-mail addresses: kmita@amu.edu.pl (H. Kmita), matteo.ceccarelli@unica.it (M. Ceccarelli), vdpbiofa@unict.it (V. De Pinto).
[1] These authors equally contributed to the work.

https://doi.org/10.1016/j.bbabio.2018.01.008
Received 13 August 2017; Received in revised form 9 January 2018; Accepted 25 January 2018
Available online 02 February 2018
0005-2728/

includes an 11-residues extension. Despite the high sequence homology and the high structural similarity [15], the three VDAC isoforms appear to be functionally different. For instance, electrophysiological experiments demonstrated that VDAC1 and VDAC2 are able to form pores in lipid bilayers [16,17], while recombinant VDAC3 turned out to have pore-forming activity, after reconstitution in artificial bilayers, with features not completely identical to the other isoforms [18,19]. Additional differences among the VDAC isoforms were detected through gene knock-out of VDAC genes [20–23].

Even if much is known about mammalian VDAC, their yeast counterparts are not as extensively characterized. Until 1997, it was believed that the single-cell organism *Saccharomyces cerevisiae* was endowed with a single VDAC gene designated *POR1*. However, Blachly-Dyson et al. noticed that deletion mutants (Δ*por*1), despite being unable to grow on glycerol media at 37 °C, were still capable to survive on the same medium at lower temperatures (30 °C) [24]. This suggested the existence of some other protein providing an alternative pathway for mitochondrial metabolites. Screening of the yeast genomic library revealed the existence of the yeast second VDAC gene, *POR2*, encoding a protein, yVDAC2, whose overexpression could correct the growth defect of Δ*por1* mutants [24]. It was immediately suspected that yVDAC2 could have different properties with respect to yVDAC1. In fact, yVDAC2 could complement the genetic defect of Δ*por1* mutants only when overexpressed, while Δ*por2* mutant did not show any impaired phenotype [24]. Finally, the double mutant Δ*por1*/Δ*por2* was still viable and able to grow on glycerol at 30 °C even if at a lower rate with respect to the Δ*por1* mutant [24]. This pattern suggested yVDAC2 to represent a less effective permeation pathway for mitochondrial metabolites with respect to yVDAC1 and it was even questioned whether yVDAC2 could fold in a channel structure at all. The importance of yVDAC2 in restoring yeast growth phenotype was confirmed by a recent study showing that transformation of yeast Δ*por*1 mutant with human Cu-Zn Superoxide Dismutase (SOD1) led to an overexpression of the *POR2* gene that results in reactivation of mitochondrial metabolism enabling the cell growth on glycerol at 37 °C [25].

In this work, we set out to perform a structural and functional characterization of yVDAC2 combining Molecular Dynamics simulations and electrophysiology. The recent disclosure of several high resolution structures of VDAC channels in mouse, human and zebrafish, all exhibiting similar sequence homology with yeast VDAC, enabled us to build homology models of yVDAC1 and yVDAC2 exploiting a multiple template approach. The channel features of the two predicted structures were analyzed and the potassium and chloride permeation pathways determined. Due to the scarce level expressed in cells, with the aim to obtain yVDAC2 amount enabling reconstitution in artificial membranes and perform electrophysiological analysis, the coding sequence of yVDAC2 was over-expressed in Δ*por1* cells and purified from LDAO solubilized isolated mitochondria. This combined approach allowed for a comprehensive description of yVDAC2 electrophysiological activity.

2. Materials and methods

2.1. Molecular dynamics simulations

Both yVDAC1 and yVDAC2 channels were embedded in a bilayer composed by 170 POPE molecules. The yVDAC1 system was bathed by a solution containing 10,358 water molecules, 96 K^+ and 97 Cl^- ions, while yVDAC2 system was solvated with 10,328 water molecules, 93 K^+ and 104 Cl^- ions. One and eleven chloride ions were respectively added to neutralize the positive charges of yVDAC1 and yVDAC2, while the other ions allowed to reach a 0.5 M concentration of *KCl*. The salt concentration is clearly higher than the physiological one, but it was chosen to enhance the number of permeation events [26]. The system first underwent 10,000 steps of conjugate gradient minimization and was then equilibrated in the NVT ensemble at 300 K. During equilibration, harmonic restraints were applied to non-hydrogen atoms of the protein backbone and side-chains as well as to the phospholipid heads. A harmonic restraint was also applied to the dihedral angle formed by Carbons 8, 9, 10, 11 of oleoyl acid and to the improper dihedral $C1 - C3 - C2 - O2$ involving the three carbons of the glycerol unit and the hydroxyl oxygen linked to its central carbon. The equilibration was organized in six stages, as detailed in Suppl. Table 1, whereby the constraints were gradually released.

After the restraints were completely relaxed, the equilibration was continued for 10 ns using a 2 fs time step. In order to enable a speed-up of the calculation, the hydrogen mass was then rescaled by a factor 4.0 which allowed to set a time-step of 4.0 fs, and the system was further equilibrated for 100 ns with this new setting. Using as input the coordinates of the last frame of this trajectory, but assigning different velocities sampled from the Maxwell-Boltzmann distribution, we performed 5 independent production runs of 100 ns each in the NVT ensemble. The last frame of three of these runs (randomly chosen) was used as input for simulations in the presence of a membrane potential. Specifically, we ran 3 simulations with a potential of +50 mV and 3 simulations with a potential of −50 mV, not far from the values used in experiments. Accordingly with literature [27], a constant external electric field $\Delta V = E * Lz$ was applied, where Lz is the dimension of the cell along the z-direction [28,29]. Currents were determined following the time-course of the charge transported across the channel and performing a linear regression of this curve. The error was estimated as the standard deviation of currents and conductances over a number of independent simulations. All simulations were performed with the Amber ff12SBildn force field [30] for the protein and the GAFFlipid force field for the lipids [31,32] using the ACEMD molecular dynamics engine [33].

Details on the analysis of ion selectivity, charge distribution calculation and permeation path identification are reported in Supplementary material.

2.2. The applied yeast Saccharomyces cerevisiae strains

The following strains were applied: M3 strain (*MATa lys2 his4 trp1 ade2 leu2 ura3*) expressing both yVDAC1 and yVDAC2, and M3-2 (*MATa lys2 his4 Δpor2::TRP1 ade2 leu2 ura3*) depleted of functional yVDAC2 (Δ*por2*). Both strains were kindly provided by prof. M. Forte (Vollum Institute for Advanced Biomedical Research, USA). Δ*por1* cells were obtained by us by introduction of kanMX4 deletion cassette into M3 cells and selected afterwards in the presence of G418.

2.3. Cloning of yeast VDAC2

The encoding sequence of yeast VDAC2 was obtained by reverse transcription from total RNA extracted from M3 *S. cerevisiae* cells. Reverse transcription was performed by using the RevertAid™ H Minus First Strand cDNA Synthesis Kit (Thermo Fisher Scientific). The corresponding cDNA was amplified by PCR, using the following primers: fw 5′–ATGAATTCATGGCACTACGATTTTTCAAC–3′; rev 5′-ATCTCGAGTC AGGGCGAGAACGATAGAGA–3′, and cloned into yeast expression vector pYX142 using *Xho*I and *Eco*RI restriction sites. The construct was verified by sequencing.

2.4. Expression and purification of yVDAC1 and yVDAC2

yVDAC1 and yVDAC2 proteins were purified from yVDAC2-depleted (Δ*por2*) and yVDAC1-depleted (Δ*por1) S. cerevisiae* cells, respectively, under native conditions. Mutant Δ*por1* cells were transformed with pYX142 expression vector containing yVDAC2 encoding sequence. The transformant cells were selected on SD-Leu selective medium (2% glucose, 0.67% Yeast Nitrogen Base, amino acids mix without leucine). The cells were grown at 28 °C in YPG medium (1% yeast extract, 2% peptone, 3% glycerol at pH 5.5). Mitochondria were

isolated as described in [34] and treated with solubilization buffer (2% LDAO, 10 mM Tris–HCl, pH 7.4) for 30 min on ice. The suspension was then loaded onto a dry hydroxyapatite:celite (2:1 *w*/w) column and elution from the column was performed with elution buffer (2% LDAO, 50 mM KCl and 10 mM Tris–HCl, pH 7.4) using the same volume as that of the column.

2.5. Electrophysiological analysis

Purified yVDAC1 and yVDAC2 were reconstituted into a planar lipid bilayer (PLB) system as previously described [19,35,42]. Bilayers of approximately 80–100 pF capacity were prepared using soybean polar lipid extract (Avanti Polar Lipids) purified before use [36], at a concentration of 25 mg/ml in *n*-decane. BLM-120 bilayer amplifier (Bio-LOGIC Science Instruments) was used, with a sampling frequency of 2 kHz, filtered at 300 Hz, and digitized using an eDAQ Chart Software. Single and multi-channel analysis, as well as voltage dependence experiments were performed in 1 M KCl, 10 mM Hepes, pH 7.0. The channel conductance (G) in symmetrical 1 M KCl was calculated from current (I) measurements at the presence of voltage *V*m of 10 mV, using equation G = I/*V*m. The voltage dependence was calculated as a ratio of G/G_0; where G denotes average conductance at a given *V*m and G_0 denotes average conductance values calculated in the presence of the lowest applied potential. Selectivity measurements were performed in 0.1 M/1 M *cis/trans* gradient of KCl and permeability ratios were calculated from the reversal potential (*V*r) using the Goldman-Hodgkin-Katz equation [37]. Channel insertion was initially achieved at symmetrical concentration of 1 M KCl (*cis/trans*). After obtaining at least 1 channel, the solution in *cis* was changed perfusing approximately 10 *chamber* volumes with 0.1 M KCl. The channel conductance in 0.1 M/1 M cis/trans gradient of KCl was calculated from the current measurements when a voltage *V*m is applied, using equation: I = G (*V*m − *V*r).

3. Results

3.1. Molecular dynamics simulations indicate similar structures but different channel features for yVDAC1 and yVDAC2

Since no crystal structure of the yeast VDACs is available, homology models were built using the MODELLERv9.15 package [38]. The overlay of the two models reported in Fig. 1A highlights their similarity quantified by a RMSD of *Cα*s of 4.08 Å. The small oscillations of the RMSD from the homology models (initial conformations) show the stability of the structures that thus retain their similarity (Fig. 1B). Despite the high similarity in terms of structure and sequence (assessed using the EMBOSS server [39] and described in Suppl. Table 2), the two yeast VDACs exhibit a significant difference in net charge both at the level of the full protein and at the level of the N-terminal end. In particular, while yVDAC1 has a positive charge +1, the net charge of yVDAC2 is +11 (see Suppl. Table 3 for a detailed charge distribution).

Simulations of currents and conductance in the structures depicted above were performed. As summarized in Fig. 2A and in Suppl. Table 4, the computation of the potassium to chloride ratio of currents and conductances, show that in the absence of a transmembrane potential there cannot be a preferential direction of the ion flow so that the average currents are close to zero, even if they change significantly from run to run, as can be deduced from the large values of the standard deviations. The direction of the current obviously depends on the sign of the potential. If the potential is positive, chloride ions preferentially move towards the negative *z*-axis while potassium ions are driven towards the positive *z*-axis. The chloride current is dominant with respect to the potassium one. Suppl. Table 4 reveals that chloride currents tend to be higher in yVDAC2 with respect to yVDAC1 while potassium currents are typically smaller. This trend is obviously mirrored by the behavior of conductances. Channel selectivity can be quantified through the absolute value of the ratio of currents or, equivalently, the absolute value of the ratio of conductances: $|g_K/g_{Cl}| = |I_K/I_{Cl}|$. Suppl. Table 4 shows that the potassium selectivity parameter in yVDAC2 is about half that in yVDAC1.

The different selectivity of yVDAC1 and yVDAC2 is reflected by the differences in their Potential of Mean Force, shown in Fig. 2B–C. In yVDAC2 the chloride PMF is characterized by two main minima at $z = -2.5$ Å and z = 7.0 Å with depth of −0.75 and −0.6 kcal/mol, respectively. In the same positions the access of K^+ ions to the channel is prevented by two barriers of 0.7 and 0.5 kcal/mol respectively. The chloride PMF in yVDAC1 is also characterized by two minima at $z = -7.0$ Å and $z = 8.0$ Å. These two minima with respective depths of −0.15 and −0.4 kcal/mol, however, are rather shallow in comparison to their counterparts in yVDAC2. In correspondence with the minima of the chloride PMF, the potassium free energy profile exhibits two modest peaks with heights of 0.15 and 0.23 kcal/mol. A third potassium peak with height of 0.20 kcal/mol is located at $z = -1.5$ Å. In short sum, in yVDAC1 the access of Cl^- ions is less favored, and the access of K^+ ions is less prevented than in yVDAC2, justifying a reduced chloride selectivity of this isoform. The different selectivity of yVDAC1 and yVDAC2 has a significant impact on the chloride and potassium permeation paths in the two channels, as shown in Figs. 3 and 4. In yVDAC2 (Fig. 3) there are four chloride permeation paths and one potassium pathway, while in yVDAC1 (Fig. 4) both Cl^- and K^+ ions cross the channel along a single path. These results appear to be consistent with the higher chloride to potassium selectivity of yVDAC2 and with the modest chloride selectivity of yVDAC1. Due to the circular symmetry of the distribution of charged residues (corresponding to the peaks and minima of the $P^+(z) - P^-(z)$ curve in Fig. 2), the chloride and potassium paths do not have a preferential placement close to specific regions of the barrel wall but tend to occupy the central part of the channels.

In Figs. 3 and 4 the beads representing the most populated ion clusters have been connected with a line in a sequence dictated by the value of the z-coordinate. Even if this choice is reasonable, obviously it is not the only possibility and alternative permeation paths could be traced. While the clustering algorithm provides an accurate estimate of the position of the most populated clusters, the possible paths connecting them are more ambiguous and any conclusion should be handled with extreme caution. In Suppl. Fig. 1 the permeation paths illustrated in Figs. 3 and 4 have been overlaid onto the axial-radial Potential of Mean Force of potassium and chloride ions. It can be noted that the proposed paths are extremely reasonable in that they connect the main free energy basins of the two-dimensional PMF. The analysis of the PMF also justifies the winding profile of potassium path in yVDAC1. The PMF in fact, shows the existence of two main free energy basins at low and high values of the radial coordinate r, so that the incoming potassium ions appear to oscillate between the two minima.

From the PMF of ions we can also estimate the conductance, as explained in ref. [29], in the small-voltage limit, and relative permeability ratio g_K/g_{Cl}, respectively 0.87 and 0.50 for yVDAC1 and yVDAC2. We obtain slightly different values with respect to the explicit current calculations, however the trend is respected, with yVDAC2 preferring anions more than yVDAC1 (see Suppl. Table 4).

We repeated the calculations using a more physiological concentration (KCl 0.15 M, 6 independent simulations of 100 ns each) and also a much higher concentration (KCl 1 M, 4 independent simulations of 100 ns each), with an external field set only at +50 mV. The conductances are plotted in the Suppl. Fig. 2. We can see how yVDAC2 shows a perfect linear conductance as a function of concentration [40] while yVDAC1 shows a small deviation from the linearity at low concentration. yVDAC2 is always more selective to anions than yVDAC1, and the selectivity is much more pronounced for yVDAC2 at low concentration (see Suppl. Table 5).

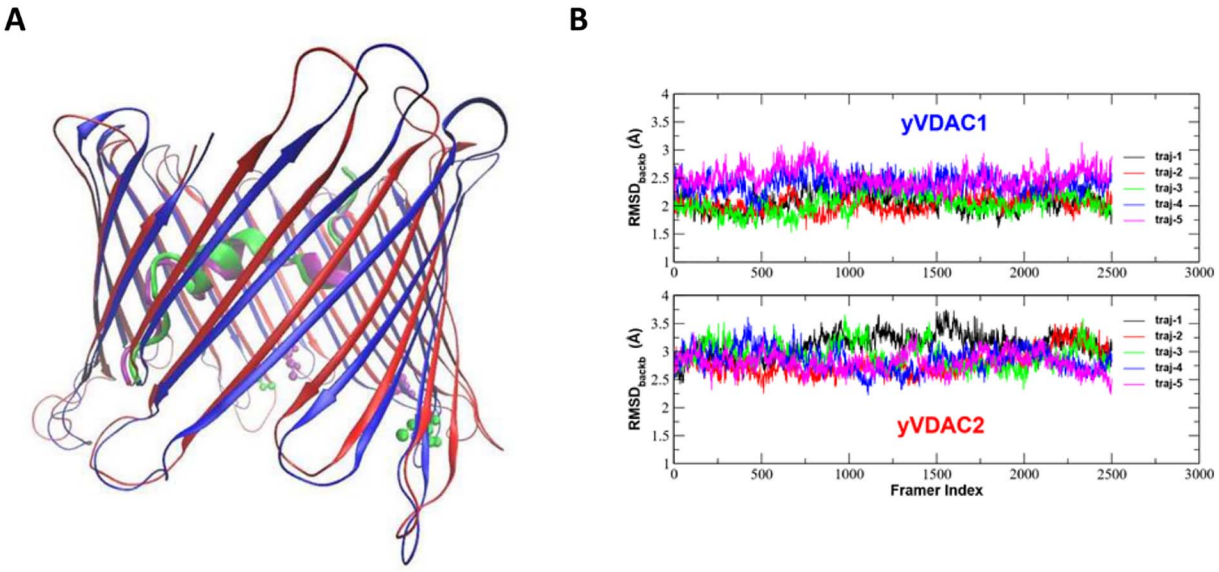

Fig. 1. Structure and stability of yVDACs.
A) Homology models of yVDAC1 (blue barrel, green N-terminal tail and cysteines 130 and 210) and yeast VDAC2 (red barrel, purple N-tail and cysteines 161 and 180). Since in all the templates, with the exclusion of the NMR structure 2K4T, the N-terminal tail is helical and leaning on the barrel wall, it is not surprising that these features are still retained by the homology models. As expected from the high level of sequence identity, the modeled structures of yVDAC1 and yVDAC2 are very similar and the RMSD computed after superposition of the C*α*s is 4.08 Å. B) Root Mean Square Deviation of backbone atoms of yVDACs. RMSD of backbone atoms of yVDAC1 and yVDAC2 with respect to the initial conformations during the five 100 ns production runs in the absence of applied electric fields. In both cases the RMSD oscillates in a narrow band (1.5–3.0 Å for yVDAC1 and 2.5–3.5 Å for yVDAC2) showing that the structures are stable and do not change significantly during the simulation.

3.2. *yVDAC2 forms channels in artificial planar lipid bilayers*

yVDAC2 is poorly expressed in yeast cells [24] and this is possibly the reason why its activity was so elusive until now. To overcome the obstacle, yeast Δ*por1* mutant cells were transformed with a plasmid encoding yVDAC2, enabling over-expression of yVDAC2. Mitochondria were isolated from transformed cells, and subjected to the classical HTP/celite purification procedure [3]. The eluate containing very tiny traces of proteins was trypsinized, and the resulting peptides analyzed by Mass Spectrometry. The analysis with the Mascot suite software allowed the identification of yVDAC2 in the eluate, showing also that no trace of yVDAC1 was present, as expected (data not shown). In parallel, yVDAC1 was purified from Δ*por2* isolated mitochondria and used herein as a control. The purified yVDAC proteins were then re-constituted into planar lipid bilayer (PLB system). The obtained traces and histograms reporting the average conductance values are shown in Fig. 5 and summarized in Table 1. It was immediately clear that yVDAC2 was able to insert into the bilayer and form channels (Fig. 5C) similar to yVDAC1 (Fig. 5A). As shown in Fig. 5D, the analysis of the yVDAC2 channel conductance, performed in 1 M KCl, 10 mM Hepes, pH 7.0, at the constant applied voltage of +10 mV, resulted in an average value of 3.57 ± 0.18 nS (SEM, n = 33) Thus, the channel average conductance was in agreement with our bioinformatic predictions (see above). Furthermore, the value was very close to the parameter value calculated for yVDAC1, i.e. 4.19 ± 0.05 nS (SEM, n = 75) (Fig. 5B). The latter is also consistent with the conductance values reported in the literature for yVDAC1 [40,42] and with other VDAC1 isoforms, like the human or *D. melanogaster* ones [43,44].

3.3. *The channel formed by yVDAC2 displays voltage dependence*

Beside channel conductance, the voltage dependence of yVDAC2 was analyzed. It is indeed known that many VDAC isoforms from different species remain in an open and high-conductive state at low potential, while at higher voltages, starting from ± 20–30 mV, the proteins switch symmetrically in several sub-closed states, characterized by lower conductance [3]. The effect of voltage value on yeast VDAC proteins' conductance was assayed in the PLB by the application of a voltage triangular wave (amplitude ± 60 mV), and the results are displayed in Fig. 6. As reported, starting from an applied voltage of ± 30 mV, yVDAC1 switched stably from high- to low-conductance states (Fig. 6A, upper curve), thus confirming the literature reports [41–44]. Data obtained for yVDAC2 indicated that the formed channels are much less voltage dependent than yVDAC1. In particular, yVDAC2 channel switched to a quite stable lower conductance state at positive potentials (+40 mV), while it continuously ran through several conductance states at negative values starting from −40 mV (Fig. 6A, lower curve). The difference in the voltage dependence between yVDAC1 and yVDAC2 is more evident in the plot shown in Fig. 6B, where the relative G/G_0 conductance is reported as a function of the applied voltage. However, the behavior of yVDAC2 closely reminded yVDAC1 voltage gating, since the former channel closure occurred at both positive and negative potentials starting from ± 40 mV, even if more pronounced at positive ones.

3.4. *Ion selectivity of yVDAC2 channel*

It is well known that VDAC shows a slight preference for anions over cations in the open state, while in the sub-closed states the channels show a slight preference for cations over anions [2,3,41]. In order to analyze the ionic selectivity of yVDAC2, the reversal potential corresponding to the voltage at zero current was measured in the presence of a 10-fold gradient of KCl. Then, the ratio between permeability of cations over anions (P_{K+}/P_{Cl-}) was calculated with the Goldman-Hodgkin-Katz equation, starting from reversal potential values. As shown in Fig. 7A, and summarized in Table 1, the current trace of a single channel formed by yVDAC1 (voltage triangular wave, amplitude ± 60 mV; frequency 10 mHz) indicated that, dependently on the applied voltage, the channel displayed two functional states characterized by different ion selectivity. At low voltages, yVDAC1 displayed the typical open state characterized by anionic selectivity and high conductance (A, anionic, in Fig. 7) whereas at high voltage, yVDAC1 switched into a closed state, characterized by cationic selectivity and low conductance (C1, cationic, in Fig. 7). Different functional states, accompanied by

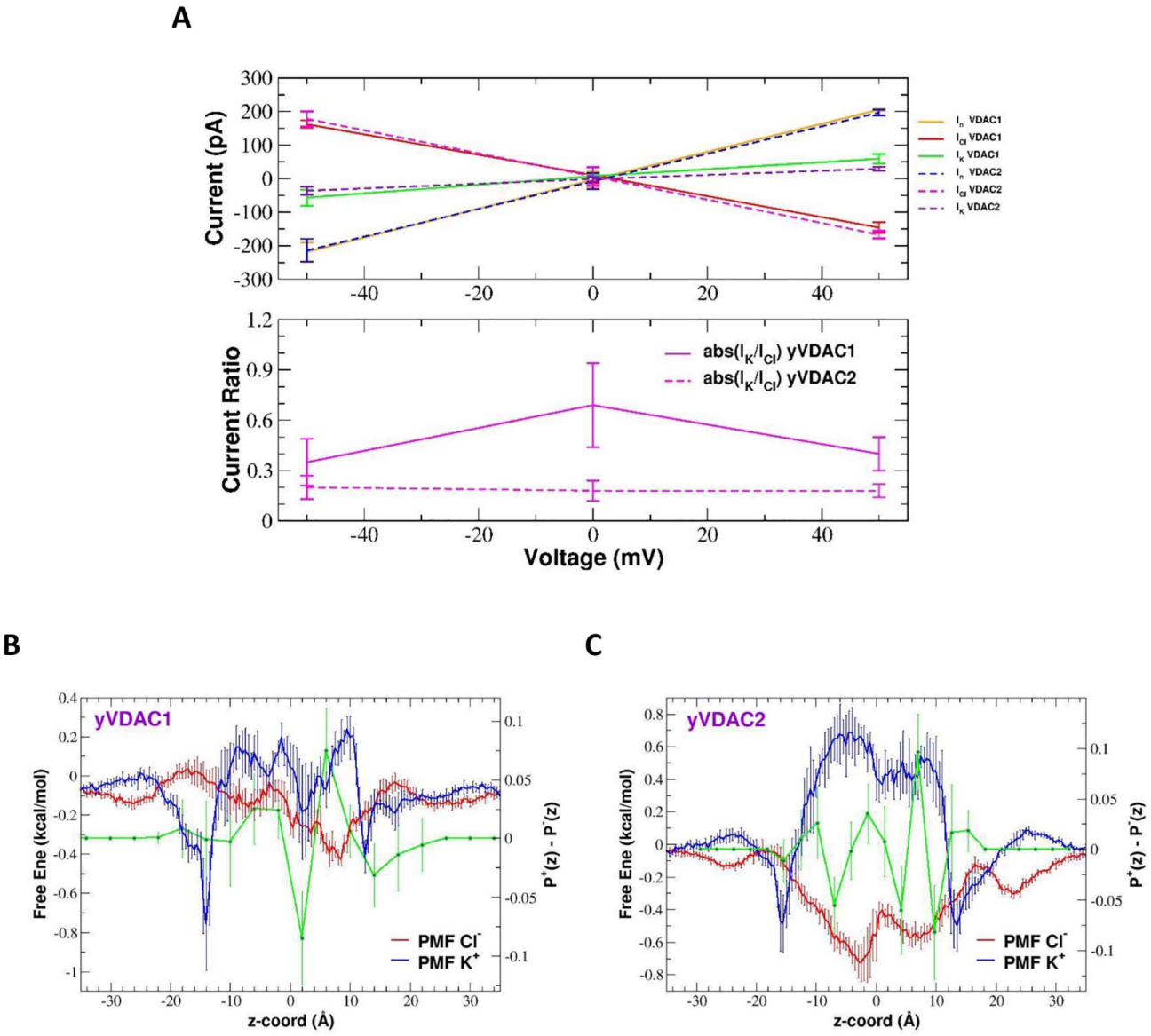

Fig. 2. Simulated currents, ion free energy profile and charge distribution in yeast VDAC pores. A) Simulated currents in yVDACs. Currents were computed using three independent trajectories at −50 mV and +50 mV and five trajectories at 0 mV. The net, chloride and potassium currents are shown in orange, red and green solid lines for yVDAC1 and in blue, magenta and violet dashed lines for yVDAC2. The lower panel is a comparison, in the two yeast VDACs, of the absolute value of the ratio of chloride to potassium currents used as selectivity indicator. B) Axial free energy profiles for chloride and potassium ions in the yVDAC1 channel. The green line shows the difference between the probability distributions of positive and negative charges. C) Axial free energy profiles for chloride and potassium ions in the yVDAC2 channel. The green line shows the difference between the probability distributions of positive and negative charges.

different ion selectivity, were observed also for yVDAC2 in a relatively short time. As shown in Fig. 7B, at low voltages, we found an anionic high-conducting state (A), definitely more anionic than the corresponding open state of yVDAC1. Application of linear regression enabled calculation of reversal potentials (Vr) (see Suppl. Fig. 3), used afterward for P_{K+}/P_{Cl^-} value calculation. As reported in Table 1, values of 0.57 ± 0.09 and 0.30 ± 0.03 were found for yVDAC1 and yVDAC2, respectively, confirming the higher anion selectivity of yVDAC2 in the open state. Moreover, with increasing voltages, two distinct cationic states were found for yVDAC2: a cationic high-conducting state (C1), resembling the C1 state of yVDAC1, and a very cationic low-conducting state (C2). Data reported in Table 1 indicate P_{K+}/P_{Cl^-} values for the two yVDAC2 cationic states of 2.17 ± 0.11 (C1) and 16.24 ± 6 (C2), respectively.

As mentioned above, ion selectivity was also predicted by means of Molecular Dynamics both using simulations with an external electric field and performing an analysis of the equilibrium PMF (Fig. 2) using the method detailed in Ref [29]. The values of P_{K+}/P_{Cl^-} computationally predicted for yVDAC1 and yVDAC2 appeared to confirm higher anionic selectivity of yVDAC2 in the open state (see Suppl. Table 4). However, it is not possible to match experimental and MD data for the others states found experimentally, since the transitions between the different functional states occur on a time-scale not accessible by current MD simulation techniques and it is important to stress that throughout our simulations the yVDAC channel always remained in the fully open state.

4. Discussion

Starting from its discovery in 1997, yVDAC2 was suspected to significantly differ from the major yeast isoform yVDAC1. In particular, since yVDAC2 compensated for the metabolic impairment of Δ*por*1 mutants only if overexpressed, and since Δ*por*2 mutants did not show any anomalous phenotype, it was suggested that yVDAC2 was unable to

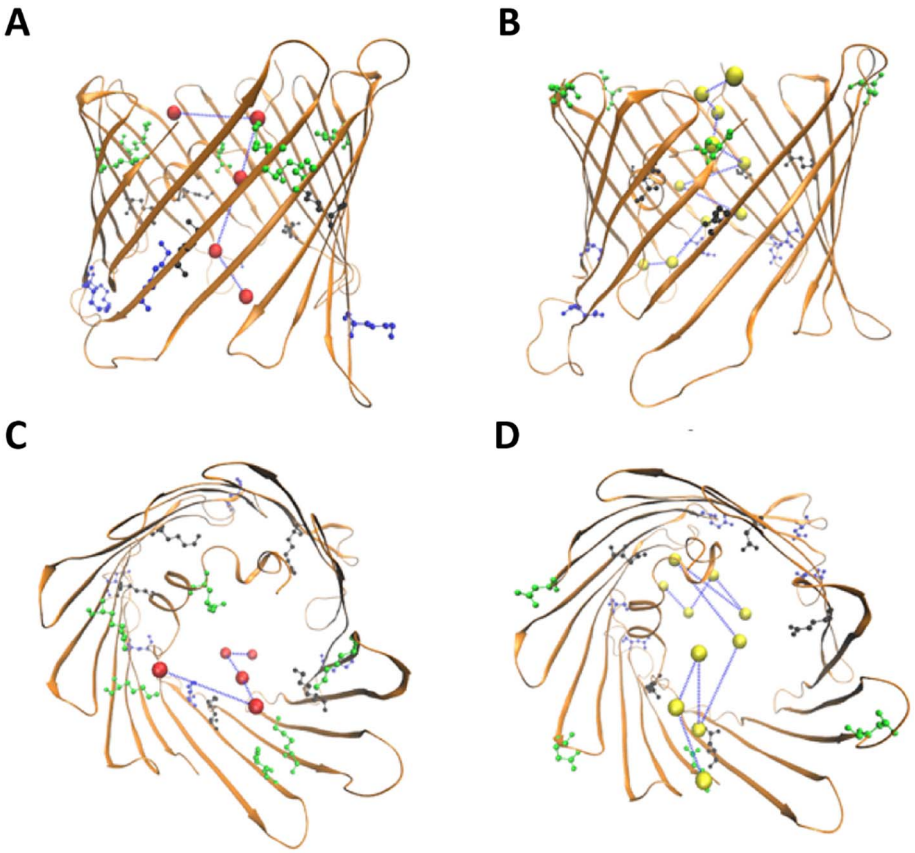

Fig. 3. Ions permeation paths in yVDAC2. Chloride (A, side view, C, top view) and potassium (B, side view, D, top view) permeation pathways in yVDAC2. In A-C the residues in blue, black and green are the Lys and Arg residues corresponding to the peaks of the $P^{+}(z) - P^{-}(z)$ curve in Fig. 2. In A–C the residues in blue (Arg80, Lys108, Lys133, Arg184) correspond to the $-20 \leq z \leq -12$ Å range; the residues in black (Lys44, Lys204, Lys234, Lys111, Arg11, Arg84, Arg124, Lys232) correspond to the $-8 \leq z \leq 4$ Å range; the residues in green (Arg4, Lys95, Arg222, Arg247) correspond to the $8 \leq z \leq 12$ Å range. In B-D the residues in blue, black and green are the Glu and Asp residues corresponding to the minima of the $P^{+}(z) - P^{-}(z)$ curve in Fig. 4. In B–D the residues in blue (Asp128, Asp134, Asp237) correspond to the $-12 \leq z \leq -8$ Å range; the residues in black (Asp8, Asp12, Asp20, Glu86) correspond to the $4 \leq z \leq 8$ Å range; the residues in green (Asp64, Asp226, Asp252) correspond to the $12 \leq z \leq 16$ Å range.

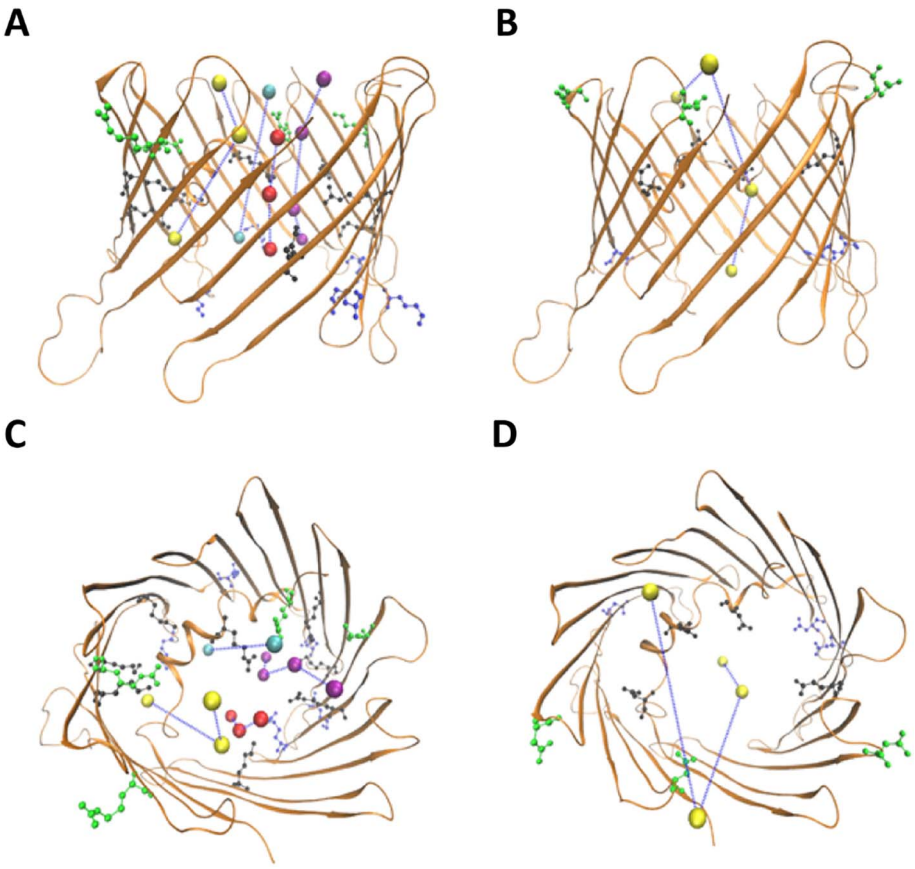

Fig. 4. Ions permeation paths in yVDAC1.
Chloride (A, side view, C, top view) and potassium (B, side view, D, top view) permeation pathways in yVDAC1. In A–C the residues in blue, black and green are the Lys and Arg residues corresponding to the peaks of the $P^{+}(z) - P^{-}(z)$ curve in Fig. 2. In A–C the residues in blue (Lys108, Lys211, Lys267, Lys46, Lys274) correspond to the $-16 \leq z \leq -8$ Å range; the residues in black (Arg164, Lys44, Lys84, Lys205, Lys236, Lys46) correspond to the $-12 \leq z \leq 0$ Å range; the residues in green (Arg11, Lys40, Lys61, Lys95, Lys248, Arg224) correspond to the $4 \leq z \leq 12$ Å range. In B–D the residues in blue, black and green are the Glu and Asp residues corresponding to the minima of the $P^{+}(z) - P^{-}(z)$ curve in Fig. 4. In B–D the residues in blue (Asp156, Glu185, Asp264, Asp128, Asp239) correspond to the $-16 \leq z \leq -8$ Å range; the residues in black (Asp20, Asp30, Lys84, Glu97, Asp139, Asp191) correspond to the $0 \leq z \leq 4$ Å range; the residues in green (Asp282, Asp64, Asp228, Asp175) correspond to the $8 \leq z \leq 20$ Å range.

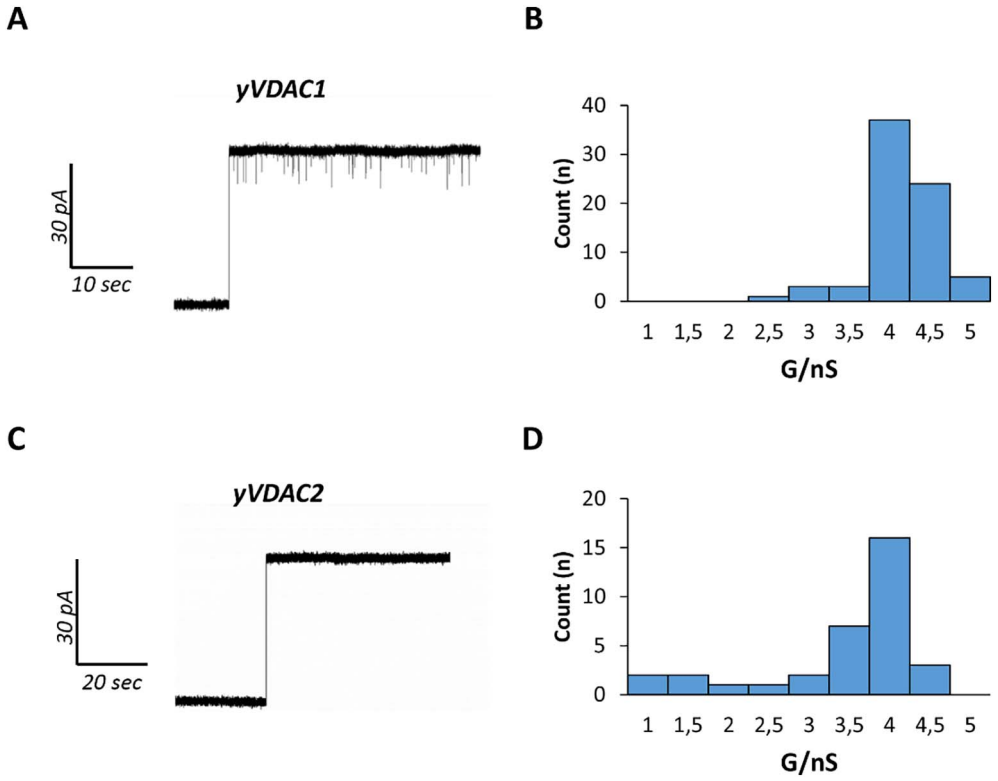

Fig. 5. Channel forming activity of yeast VDAC proteins.
Representative traces of single-channel recordings for yVDAC1 (A) and yVDAC2 (C). The experiments were performed in 1 M KCl, 10 mM Hepes, pH 7.0, at the constant voltage of +10 mV. Histograms showing the calculated conductance values for yVDAC1 (n = 75) (B) and for yVDAC2 (n = 33) (D).

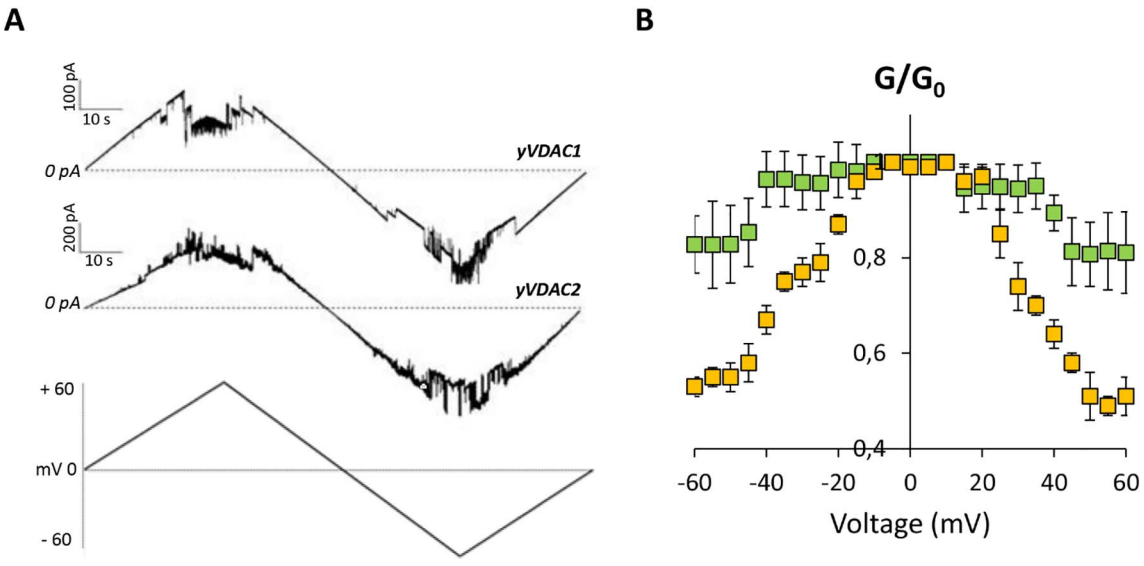

Fig. 6. Voltage dependence of channels formed by yeast VDAC proteins.
A) Channel conductance analysis in the presence of voltage triangular curve recorded between ± 60 mV. The upper curve refers to yVDAC1 (n = 2 channels) and resembles literature reports. The lower curve refers to yVDAC2 (n = 4 channels). The yVDAC2 closure starts from ± 40 mV. B) Analysis of G/G_0 ratio (± SEM) showing the different voltage dependence features of yVDAC proteins. At least three independent experiments were performed for each protein. Yellow squares refer to yVDAC1, while green squares refer to yVDAC2.

form channels in either bilayers or liposomes [24,44]. Direct information about the gene and the protein are astonishingly rare. Interestingly, a Meeting report [46] indicated that yVDAC2 could have a role in the transport of tRNAs from cytosol into mitochondria and that this role is exerted also by other barrel-forming proteins like Tom40 and yVDAC1. In another recent report in a Meeting [47], the whole proteome appearing on SDS-PAGE of purified yeast outer membrane did not show the presence of yVDAC2. At the end, in a recent work, it was serendipitously found that the appearance of yVDAC2 was stimulated by the addition of an external factor, in that case the human SOD1 [25]. The same expression stimulation could not be associated to the overexpression of yeast SOD1 [25]. All together, these intriguing data pushed us to clarify the real functional features of the protein and to try to understand more about the reason of its presence in *S. cerevisiae* mitochondria.

Sequence comparison supported the construction of yVDACs

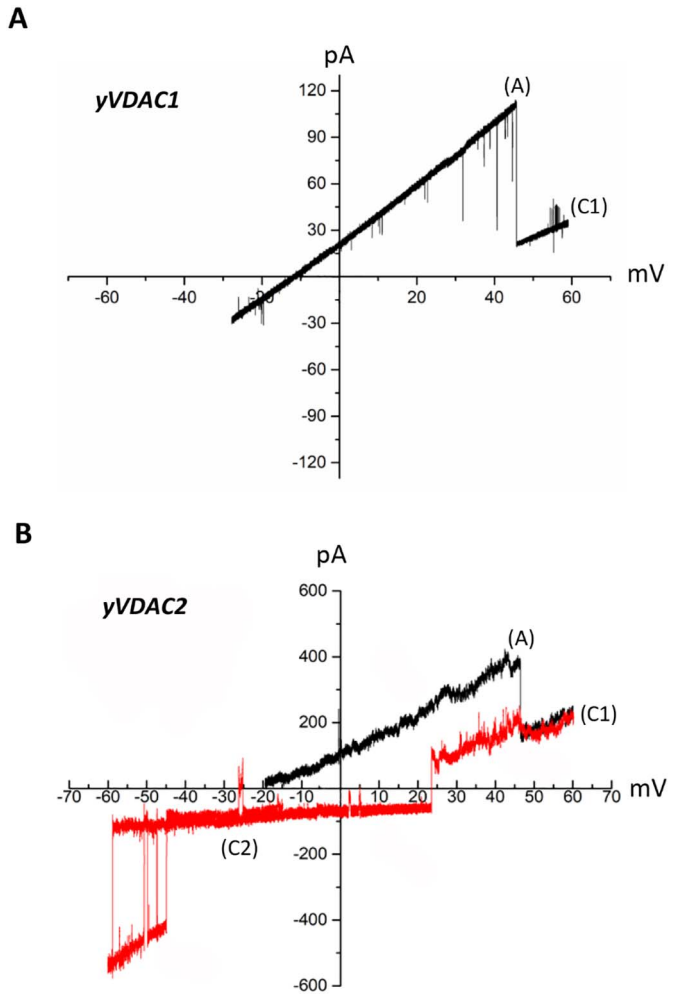

Fig. 7. Ionic selectivity of channels formed by yeast VDAC proteins.
A) Representative trace of yVDAC1 obtained by application of voltage triangular wave (amplitude ± 60 mV) performed with n = 1 channel inserted in the membrane. Trace shows two different functional states, corresponding to the canonical "open" anion high-conducting state at low voltages (anionic, A) and "close" cationic low-conducting state at high voltages (cationic, C1). B) Representative trace of yVDAC2 obtained by application of voltage triangular wave (amplitude ± 60 mV). Different colors were used to indicate different functional states. Experiment was performed with n = 2 channels inserted in the membrane. Black curve refers to the anionic high-conducting selective state (A), whereas red curve refers to two cationic states, named respectively cationic 1 (C1) and cationic 2 (C2).

structures. Molecular modeling suggested a putative structure for the two yVDAC isoforms akin to mammalian VDAC1 and zebrafish VDAC2. Thus, yVDAC2 appeared to have pore-size and channel availability to ions and metabolites similar to those found in "classical" pores like mammalian VDACs. To verify these observations we decided to directly probe the function of the pore after reconstitution in artificial membranes. Therefore, Δ*por*1 strain was transformed with a centromeric plasmid carrying the yVDAC2 sequence, to enhance the number of transcribed genes and consequently the protein expression level. Then, yVDAC2 protein was purified from a detergent-extracted, purified mitochondrial fraction. This strategy enabled to overcome the very low expression level of yVDAC2 also found by Blachy-Dyson et al. [24] and reported by Pfanner [47]. Our results clearly demonstrated that yVDAC2 is able to form channels with conductance values essentially similar to yVDAC1, used in this study as control, and to that of the most studied mammalian VDACs [1–3,41–44]. Both channels are also able to close in the presence of a raised applied voltage although we found some differences in the voltage-dependence of the two isoforms. Nevertheless, the voltage-dependence indicates that also yVDAC2 displays this typical feature of the eukaryotic porins.

A more complex pattern was noticed for the ionic selectivity. The bioinformatics analysis predicted a clear anion selectivity for yVDAC2 in open state, higher than for yVDAC1 open state. This was first suspected from the significant difference in the net charge between yVDAC1 (+1) and yVDAC2 (+11). The parameters evaluated by computations showed that the chloride selectivity of yVDAC2 is two to three times higher than that of yVDAC1. Consistently, it was found that in yVDAC2 there are four chloride permeation pathways and one potassium pathway while in yVDAC1 both chloride and potassium ions cross the channel along a single, though different, path. Moreover, the analysis of the PMF as a function of the axial position, revealed that in yVDAC1 the access of Cl^- ions is less favored and the access of K^+ ions is less prevented than in yVDAC2. Reconstitution experiments set in a planar lipid bilayer apparatus show some slight difference from computations. In particular, the anionic high-conducting state displayed by yVDAC2 is definitely more anionic than the corresponding state of yVDAC1. On the other hand, the KCl gradient between two sides of the membrane resulted in shifts in the current/voltage curve slope, allowing for identification of up to three different states with different calculated parameters of ionic selectivity for yVDAC2. Interestingly, two of them appear to be high-conductance states but with opposite selectivity, as previously observed for VDAC1 [48].

Anyway, the slight differences between the electrophysiological results and the computed information, are probably due to unpredictable differences in the protein conformation. In addition, incorporation of yVDAC2 in the artificial membrane is not as easy as for the classical mammalian VDAC1 and can cause additional bias to the final results. However, difficulties in channel insertion into planar bilayer or liposomes is not unusual in the VDAC family. For instance, until recently, all attempts to characterize hVDAC3 channel activity were unsuccessful since its insertion in artificial membranes was observed very rarely, only after the addition of large amounts of reducing agents [49]. Only recently Checchetto and coworkers discovered that human VDAC3 forms low-conductance channels that until then had been unnoticed [18,19] in addition to pores of "canonical" size [19,42]. Thus, it could not be excluded that yVDAC2 insertion could be very sensitive to the pH of the medium [50] or to the presence of reducing agents: such modifications might exert an influence on the process that yVDAC2 polypeptide sustain to reach the transmembrane conformation during

Table 1
Summary of the electrophysiological features of yeast VDAC proteins.
An overview of conductance, voltage dependence and ion selectivity parameters experimentally determined for yeast VDAC proteins. Values of permeability of purified yVDAC1 and yVDAC2 proteins were calculated from the reversal potential obtained by linear regression as in Suppl. Fig. 2. As explained in description of Fig. 7, (A) refers to anionic high-conducting state, (C1) refers to cationic low-conducting state and (C2) refers to the very cationic low-conducting state. In parenthesis, values of conductance calculated for the different states in 0.1 M/1 M KCl gradient.

	Average conductance (nS)	Voltage dependence	P_K/P_{Cl} (A) (nS)	P_K/P_{Cl}(C1) (nS)	P_K/P_{Cl}(C2) (nS)
yVDAC1	4.19 ± 0.05	> ± 30 mV	0.57 ± 0.09 (2.04 ± 0.19)	3.9 ± 0.4 (1.1 ± 0.1)	–
yVDAC2	3.57 ± 0.18	> ± 40 mV	0.30 ± 0.03 (1.49 ± 0.09)	2.17 ± 0.11 (1.9 ± 0.08)	16.24 ± 6 (0.33 ± 0.06)

the membrane insertion process [24,45]. Our results, obtained with two different approaches and despite the slight differences outlined in the text, give the definitive message that yVDAC2 is another member of the VDAC family.

What is the role of yVDAC2 in the yeast? As for yVDAC1, the protein appears to contribute to metabolite transport across the mitochondrial outer membrane [51]. It has also been shown that, like yVDAC1, yVDAC2 is important for intracellular reduction-oxidation (redox) states as determined for mitochondria and cytosol fractions [52]. Surprisingly, yVDAC2 is not able to reverse the phenotype of yeast mutant depleted of yVDAC1, as shown by the growth defect of the Δ*por*1 strain [24]. In conclusion the protein could supplement but not substitute yVDAC1, as the result of a different gene-expression control. This is further supported by the transformation of Δ*por*1 with SOD1 expressing plasmids [25]. While the overexpression of the endogenous yeast SOD1 does not change the yVDAC2 expression level in the cell, the overexpression of the human SOD1 (hSOD1) does [25]. The latter indeed, probably acting as a transcription factor [53], enhances the expression levels of genes encoding mitochondrial outer membrane proteins, including *POR2*, that could compensate for the lack of yVDAC1 [25]. Nevertheless, the failure of hSOD1 to restore the normal growth phenotype of Δ*por*1Δ*por*2 double mutant highlighted the central role of yVDAC2 in the effect of hSOD1 [25].

The expression of human hSOD1 is not physiological but can indicate that a completely external factor is necessary to influence the machinery controlling the yVDAC2 gene, ultimately causing an improvement in its expression. The extraordinary signals able to enhance yVDAC2 expression in the *S. cerevisiae* have not been found yet. A final explanation of the physiology and molecular biology of yVDAC2 will come only from studies of the gene control region and from the localization of the trans-acting molecule(s) causing such a specific control.

Transparency document

The Transparency document associated with this article can be found, in online version.

Acknowledgments

The authors acknowledge the financial support of MIUR PRIN, project 2015795S5W_005, and Fondazione Umberto Veronesi for a post-doctoral fellowship to A. Magrì. M.C. thanks the project RAS/FdS (CUP F72F16003070002).

Authors contributions

C.G. and I.B. performed MD simulations, A. Magrì, M.C.D.R., A.K. and S.R. performed experiments, A. Messina, V.D.P., H.K. and M.C. designed the research. All the authors contributed to write the manuscript.

Competing financial interests statement

The authors declare no competing financial interests.

Appendix A. Supplementary data

Supplementary data to this article can be found online at https://doi.org/10.1016/j.bbabio.2018.01.008.

References

[1] R. Benz, Permeation of hydrophilic solutes through mitochondrial outer membranes: review on mitochondrial porins, Biochim. Biophys. Acta 1197 (1994) 167–196.
[2] M. Colombini, VDAC: the channel at the interface between mitochondria and the cytosol, Mol. Cell. Biochem. 256–257 (2004) 107–115.
[3] V. Shoshan-Barmatz, V. De Pinto, M. Zweckstetter, Z. Raviv, N. Keinan, N. Arbel, VDAC, a multi-functional mitochondrial protein regulating cell life and death, Mol. Asp. Med. 31 (2010) 227–285.
[4] A. Messina, S. Reina, F. Guarino, V. De Pinto, VDAC isoforms in mammals, Biochim. Biophys. Acta 1818 (2012) 1466–1476.
[5] M.J. Young, D.C. Bay, G. Hausner, D.A. Court, The evolutionary history of mitochondrial porins, BMC Evol. Biol. 7 (2007) 1–21.
[6] E. Blachly Dyson, S. Peng, M. Colombini, M. Forte, Selectivity changes in site-directed mutants of the VDAC ion channel: structural implications, Science 247 (1990) 1233–1236.
[7] J. Song, C. Midson, E. Blachy-Dyson, M. Forte, M. Colombini, The sensor regions of VDAC are translocated from within the membrane to the surface during the gating processes, Biophys. J. 74 (1998) 2926–2944.
[8] R. Casadio, I. Jacoboni, A. Messina, V. De Pinto, A 3D model of the voltage-dependent anion channel (VDAC), FEBS Lett. 520 (2002) 1–7.
[9] S. Hiller, R.G. Graces, T.J. Malia, V.Y. Orekhov, M. Colombini, G. Wagner, Solution structure of the integral human membrane protein VDAC-1 in detergent micelles, Science 321 (2008) 1206–1210.
[10] M. Bayrhuber, T. Menis, M. Habeck, S. Becker, K. Giller, S. Villinger, C. Vonrhein, C. Griesinger, M. Zweckstetter, K. Zeth, Structure of the human voltage-dependent anion channel, Proc. Natl. Acad. Sci. U. S. A. 105 (2008) 15370–15375.
[11] R. Ujwal, D. Cascio, J.P. Colletier, S. Fahama, J. Zhanga, L. Torod, P. Pinga, J. Abramson, The crystal structure of mouse VDAC1 at 2.3 Å resolution reveals mechanistic insights into metabolite gating, Proc. Natl. Acad. Sci. U. S. A. 105 (2008) 17742–17747.
[12] G. Schulz, Beta-barrel membrane proteins, Curr. Opin. Struct. Biol. 10 (2000) 443–447.
[13] B. van den Berg, S. Prathyusha Bhamidimarri, J. Dahyabhai Prajapati, U. Kleinekathöfer, M. Winterhalter, Outer-membrane translocation of bulky small molecules by passive diffusion, Proc. Natl. Acad. Sci. U. S. A. 112 (2015) E2991–9.
[14] J. Schredelseker, A. Paz, C.J. López, C. Altenbach, C.S. Leung, M.K. Drexler, J.N. Chen, W.L. Hubbell, J. Abramson, High resolution structure and double electron-electron resonance of the zebrafish Voltage-dependent Anion Channel 2 reveal an oligomeric population, J. Biol. Chem. 289 (2014) 12566–12577.
[15] G.F. Amodeo, M.A. Scorciapino, A. Messina, V. De Pinto, M. Ceccarelli, Charged residues distribution modulates selectivity of the open state of human isoforms of the Voltage Dependent Anion-selective Channel, PLoS One 9 (2014) e103879.
[16] G. Bàthori, I. Szabo, I. Schmehl, F. Tombola, V. De Pinto, M. Zoratti, Novel aspects of the electrophysiology of mitochondrial porin, Biochem. Biophys. Res. Commun. 243 (1998) 258–263.
[17] V. Menzel, M.C. Cassará, R. Benz, V. De Pinto, A. Messina, V. Cunsolo, R. Saletti, K.D. Hinsch, E. Hinsch, Molecular and functional characterization of VDAC2 purified from mammal spermatozoa, Biosci. Rep. 29 (2009) 351–362.
[18] V. Checchetto, S. Reina, A. Magrì, I. Szabò, V. De Pinto, Recombinant human voltage dependent anion selective channel isoform 3 (hVDAC3) forms pores with a very small conductance, Cell. Physiol. Biochem. 34 (2014) 842–853.
[19] S. Reina, V. Checchetto, R. Saletti, A. Gupta, D. Chaturvedi, C. Guardiani, F. Guarino, M.A. Scorciapino, A. Magrì, S. Foti, M. Ceccarelli, A. Messina, R. Mahalakshmi, I. Szabo, V. De Pinto, VDAC3 as a sensor of oxidative state of the intermembrane space of mitochondria: the putative role of cysteine residue modifications, Oncotarget 7 (2016) 2249–2268.
[20] S. Wu, M.J. Sampson, W.K. Decker, W.J. Craigen, Each mammalian mitochondrial outer membrane porin protein is dispensable: effects on cellular respiration, Biochim. Biophys. Acta 1452 (1999) 68–78.
[21] K. Anflous, D.D. Armstrong, W.J. Craigen, Altered mitochondrial sensitivity for ADP and maintenance of creatine-stimulated respiration in oxidative striated muscles from VDAC1-deficient mice, J. Biol. Chem. 276 (2001) 1954–1960.
[22] M.J. Sampson, W.K. Decker, A.L. Beaudet, W. Ruitenbeek, D. Armstrong, M.J. Hicks, W.J. Craigen, Immotile sperm and infertility in mice lacking mitochondrial voltage dependent anion channel type 3, J. Biol. Chem. 276 (2001) 39206–39212.
[23] E.H. Cheng, T.V. Sheiko, J.K. Fisher, W.J. Craigen, S.J. Korsmeyer, VDAC2 inhibits BAK activation and mitochondrial apoptosis, Science 301 (2003) 513–517.
[24] E. Blachly-Dyson, J. Song, W.J. Wolfgang, M. Colombini, M. Forte, Multicopy suppressors of phenotypes resulting from the absence of yeast VDAC encode a VDAC-like protein, Mol. Cell. Biol. 17 (1997) 5727–5738.
[25] A. Magrì, M.C. Di Rosa, M.F. Tomasello, F. Guarino, S. Reina, A. Messina, V. De Pinto, Overexpression of human SOD1 in VDAC1-less yeast restores mitochondrial functionality modulating beta-barrel outer membrane protein genes, Biochim. Biophys. Acta 1857 (2016) 789–798.
[26] M.B. Ulmschneider, C. Bagneris, E.C. McCusker, P.G. DeCaen, M. Delling, D.E. Clapham, J.P. Ulmschneider, B.A. Wallace, Molecular dynamics of ion transport through the open conformation of a bacterial voltage-gated sodium channel, Proc. Natl. Acad. Sci. U. S. A. 110 (16) (2013) 6363–6364.
[27] J. Gumbart, F. Khalili-Araghi, M. Sotomayor, B. Roux, Constant electric field simulations of the membrane potential illustrated with simple systems, Biochim. Biophys. Acta 1818 (2012) 294–302.
[28] S. Samanta, M.A. Scorciapino, M. Ceccarelli, Molecular basis of substrate translocation through the outer membrane channel OprD of *Pseudomonas aeruginosa*, Phys. Chem. Chem. Phys. 17 (2015) 23867–23876.
[29] I. Ghai, A. Pira, M.A. Scorciapino, I. Bodrenko, L. Benier, M. Ceccarelli, M. Winterhalter, R. Wagner, General method to determine the flux of charged molecules through nanopores applied to β-Lactamase inhibitors and OmpF, J. Phys. Chem. Lett. 8 (2017) 1295–1301.
[30] K. Lindorff-Larsen, S. Piana, K. Palmo, P. Maragakis, J.L. Klepeis, R.O. Dror,

D.E. Shaw, Improved side-chain torsion potentials for the Amber ff99SB protein force field, Proteins 78 (2010) 1950–1958.
[31] C. Dickson, L. Rosso, R. Betz, R. Walker, I. Gould, GAFFlipid: a general Amber Force Field for the accurate molecular dynamics simulation of phospholipid, Soft Matter 8 (2012) 9617–9627.
[32] J. Domanski, P. Stansfeld, M. Sansom, O. Beckstein, Lipidbook: a public repository for forcefield parameters used in membrane simulations, J. Membr. Biol. 236 (2010) 255–258.
[33] M. Harvey, G. Giupponi, G. De Fabritiis, ACEMD: accelerating biomolecular dynamics in the microsecond time scale, J. Chem. Theory Comput. 5 (2009) 1632–1639.
[34] G. Daum, S.M. Gasser, G. Schatz, Import of proteins into mitochondria. Energy-dependent, two-step processing of the intermembrane space enzyme cytochrome b2 by isolated yeast mitochondria, J. Biol. Chem. 257 (1982) 13075–13080.
[35] A. Magrì, R. Belfiore, S. Reina, M.F. Tomasello, M.C. Di Rosa, F. Guarino, L. Leggio, V. De Pinto, A. Messina, Hexokinase I N-terminal based peptide prevents the VDAC1-SOD1 G93A interaction and re-establishes ALS cell viability, Sci. Rep. 6 (2016) 34802.
[36] W. Hanke, W.R. Schlue, Planar lipid bilayers: methods and applications, London New York: Acad. Press 47 (1993).
[37] E.M. Krammer, H. Saidani, M. Prévost, F. Homblé, Origin of ion selectivity in *Phaseolus coccineus* mitochondrial VDAC, Mitochondrion 19 (2014) 206–213.
[38] A. Sali, T.J. Blundell, Comparative protein modelling by satisfaction of spatial restraints, Mol. Biol. 234 (1993) 779–815.
[39] P. Rice, I. Longden, A. Bleasby, EMBOSS: the European molecular biology open software suite, Trends Genet. 16 (2000) 276–277.
[40] E.M. Krammer, F. Homblé, M. Prévost, Concentration dependent ion selectivity in VDAC: a molecular dynamics simulation study, PLoS One 6 (2011) e27994.
[41] R. Benz, A. Schmid, M. Dihanich, Pores from mitochondrial outer membranes of yeast and a porin-deficient yeast mutant: a comparison, J. Bioenerg. Biomembr. 21 (1898) 439–450.
[42] A. Karachitos, D. Grobys, M. Antoniewicz, S. Jedut, J. Jordan, H. Kmita, Human VDAC isoforms differ in their capability to interact with minocycline and to contribute to its cytoprotective activity, Mitochondrion 28 (2016) 38–48.
[43] S. Reina, A. Magrì, M. Lolicato, F. Guarino, A. Impellizzari, E. Maier, R. Benz, M. Ceccarelli, V. De Pinto, A. Messina, Deletion of β-strands 9 and 10 converts VDAC1 voltage-dependence in an asymmetrical process, Biochim. Biophys. Acta 1827 (2013) 793–805.
[44] V. De Pinto, R. Benz, C. Caggese, F. Palmieri, Characterization of the mitochondrial porin from *Drosophila melanogaster*, Biochim. Biophys. Acta 987 (1989) 1–7.
[45] A.C. Lee, X. Xu, E. Blachly-Dyson, M. Forte, M. Colombini, The role of yeast VDAC genes on the permeability of the mitochondrial outer membrane, J. Membr. Biol. 161 (1998) 173–181.
[46] M.Y. Vyssokikh, T. Schirtz, O. Kolesnikova, N. Entelis, Y.N. Antonenko, T.I. Rokitskaya, I. Tarassov, Isoform porin 2 is involved in tRNALys transport from cytosol to mitochondria in yeast, Biochim. Biophys. Acta 1817 (2012) S124–S125.
[47] N. Pfanner, Mitochondrial machineries for import and assembly of proteins, Biochim. Biophys. Acta 1857 (2016) e4.
[48] E. Pavlov, S.M. Grigoriev, L.M. Dejean, C.L. Zweihorn, C.A. Mannella, K.W. Kinnally, The mitochondrial channel VDAC has a cation-selective open state, Biochim. Biophys. Acta 1710 (2005) 96–102.
[49] M. Colombini, The VDAC channel: molecular basis for selectivity, Biochim. Biophys. Acta 1863 (2016) 2498–2502.
[50] O. Teijido, S.M. Rappaport, A. Chamberlin, S.Y. Noskov, V.M. Aguilella, T.K. Rostovtseva, S.M. Bezrukov, Acidification asymmetrically affects voltage-dependent anion channel implicating the involvement of salt bridges, J. Biol. Chem. 289 (2014) 23670–23682.
[51] N. Antos, M. Budzińska, H. Kmita, An interplay between the TOM complex and porin isoforms in the yeast *Saccharomyces cerevisiae* mitochondria, FEBS Lett. 500 (2001) 12–16.
[52] H. Galganska, M. Budzinska, M. Wojtkowska, H. Kmita, Redox regulation of protein expression in *Saccharomyces cerevisiae* mitochondria: possible role of VDAC, Arch. Biochem. Biophys. 479 (2008) 39–45.
[53] C. Tsang, Y. Liu, J. Thomas, Y. Zhang, X. Zheng, Superoxide dismutase 1 acts as a nuclear transcription factor to regulate oxidative stress resistance, Nat. Commun. 5 (2014) 3446.